JACS
JOURNAL OF THE AMERICAN CHEMICAL SOCIETY
Article
pubs.acs.org/JACS

In Situ Optical and Structural Studies on Photoluminescence Quenching in CdSe/CdS/Au Heterostructures

Arnaud Demortière,[†,▽] Richard D. Schaller,[*,†,○] Tao Li,[§] Soma Chattopadhyay,[#,▽] Galyna Krylova,[†] Tomohiro Shibata,[#,▽] Paula C. dos Santos Claro,[†] Clare E. Rowland,[○] Jeffrey T. Miller,[∥] Russell Cook,[⊥] Byeongdu Lee,[§] and Elena V. Shevchenko[*,†]

[†]Center for Nanoscale Materials, [‡]Materials Science Division, [§]Advanced Photon Source, [∥]Chemical Sciences and Engineering Division, [⊥]Electron Microscopy Center, Argonne National Laboratory, 9700 South Cass Ave., Argonne, Illinois 60439, United States
[#]CSRRI-IIT, MRCAT, Sector 10, Bldg 433B, Argonne National Laboratory, Argonne, Illinois 60439, United States
[▽]Physics Department, Illinois Institute of Technology, Chicago, Illinois 60616, United States
[○]Department of Chemistry, Northwestern University, 2145 Sheridan Rd., Evanston, Illinois 60208, United States

Supporting Information

ABSTRACT: We report here detailed in situ studies of nucleation and growth of Au on CdSe/CdS nanorods using synchrotron SAXS technique and time-resolved spectroscopy. We examine structural and optical properties of CdSe/CdS/Au heterostructures formed under UV illumination. We compare the results for CdSe/CdS/Au heterostructures with the results of control experiments on CdSe/CdS nanorods exposed to gold precursor under conditions when no such heterostructures are formed (no UV illumination). Our data indicate similar photoluminescence (PL) quenching and PL decay profiles in both types of samples. Via transient absorption and PL, we show that such behavior is consistent with rapid (faster than 3 ps) hole trapping by gold−sulfur sites at the surface of semiconductor nanoparticles. This dominant process was overlooked in previous end-point studies on semiconductor/metal heterostructures.

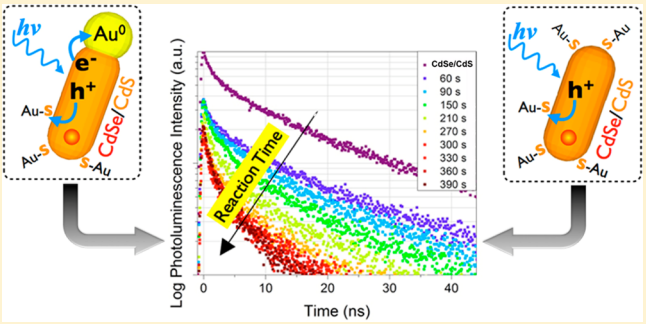

INTRODUCTION

Hybrid nanoparticles (NPs)[1−6] are promising candidates in many technologically important areas such as solar energy conversion[7] and catalysis.[8] In particular, heterostructures of metal and semiconductor NPs are of interest for the design of next generation photovoltaic and electronic devices due to their reported semiconductor-to-metal photoinduced charge separation properties.[9−12] Furthermore, shifting of the metal Fermi level closer to the conduction band of semiconductor NPs can improve charge separation and yield more reductive potential,[13] for example, facilitating the photoinduced water splitting.[1,14−17] Moreover, the formation of semiconductor/metal heterostructures (e.g., CdS/Au) leads to the modification of the absorption spectra and the extension of quantum confinement.[18]

Detailed understanding of the interactions between constituents in multicomponent heterostructures is critical for further progress in material design and establishing structure−property correlations.[19−21] The combination of quantum confinement effects and plasmonic effects in semiconductor/noble metal heterostructures can lead to enhanced or quenched photoluminescence (PL) depending on energy and charge transfer processes. For instance, in end-point (no in situ) studies on CdS/Au heterostructures ultrafast electron transfer (<20 fs) from CdS to Au was found to quench the PL and led to a red-shift of the surface plasmon resonance.[22] Also recent studies on CdS/Pt heterostructures also suggest ultrafast (∼3.4 ps) electron transfer from CdS to Pt leading to PL quenching while the charge recombination was significantly slower (∼1.2 μs) assuming the hole trapping in semiconductor part.[1] Conversely, Zamkov et al. reported that the PL quenching in CdS/Au heterostructures is a result of ultrafast carrier trapping at interfacial states, since PL quenching was, in fact, faster than the electron transfer from CdS to Au.[23] It has been shown that charge transfer can also depend on the presence of hole and electron scavengers, that further allows improved performance of the photocatalytic systems.[17]

Understanding charge transfer processes is important for design of efficient catalysts[24,25] and PL quenching can be utilized for chemical sensing[26,27] since PL quenching is very sensitive to a large range of adsorbates such as capping ligands, polymers, and metallic ions.[28−30]

Despite many studies focused on semiconductor/metal heterostructures,[10,31,32] previous efforts were focused on analysis of optical properties of the formed (end-point) semiconductor/noble metal heterostructures and did not follow

Received: September 6, 2013
Published: January 21, 2014

   dx.doi.org/10.1021/ja4092616 | J. Am. Chem. Soc. 2014, 136, 2342−2350

the changes of optical and structural properties during formation of such structures. Herein, we report in situ evolution of optical and structural properties of CdSe/CdS nanorods as a result of their reaction with gold precursor with and without UV illumination (further referred to as UV and no-UV samples) using synchrotron X-ray scattering and spectroscopic techniques. As expected,[22] UV illumination of the reaction mixture containing semiconductor NPs and gold precursor resulted in nucleation and growth of a Au domain at the tip of CdSe/CdS nanorod, while no formation of Au domains was observed without UV illumination. Nevertheless we observe remarkably similar PL quenching and PL decay profiles in UV and no-UV samples. We report that quenching takes place even without formation of distinct Au domains at CdSe/CdS nanorods. Our in situ study of evolution of optical properties as a function of reaction time during nucleation and growth of Au domains on CdSe/CdS nanorods provide important insights into understanding of charge separation processes of semiconductor/metal heterostructures that are of a great interest in light-harvesting and sensing applications.

EXPERIMENTAL SECTION

Materials. CdO (Sigma-Aldrich, 99%), *n*-propylphosphonic acid (PPA, Sigma-Aldrich, 95%), trioctylphosphine oxide (TOPO, Sigma-Aldrich, 99%), octadecylphosphonic acid (ODPA, PCI Synthesis, 97%), trioctylphosphine (TOP, Fluka, 90%), selenium (Aldrich, 98%), sulfur (Sigma-Aldrich, 99%), *n*-propylphosphonic acid (PPA, Aldrich, 95%), dodecylamine (Sigma-Aldrich, 99%), dodecanoic acid (Sigma-Aldrich, 99%), octylamine (Aldrich, 99%), $AuCl_3$ (Aldrich, 90%), and DDAB (Sigma Aldrich 98%) were used for the synthesis of golden-tipped CdSe/CdS nanorods. The chemicals were used as received.

Synthesis of CdSe Seeds. CdSe seeds (2 nm) were synthesized by using 50 mL three-neck flask and Schlenk-line approach.[33] TOPO (3.0 g), ODPA (0.308 g), and CdO (0.060 g) were mixed, heated up to 150 °C, and kept under vacuum for 2 h. The reaction solution was then heated up under nitrogen to 300 °C at approximately 7 °C/min. The reaction solution became transparent, indicating the formation of Cd-ODPA complexes. Next, 1.5 g of TOP was rapidly injected into the reaction flask. After that TOP-Se solution (0.058 g Se + 0.360 g TOP) was injected at 380 °C. The reaction was quenched immediately after the injection of TOP-Se by injection of 5 mL of room-temperature toluene. After the solution was cooled down to room temperature, the CdSe seeds were precipitated by adding ethanol and centrifuging. This washing step was repeated twice. Finally, the seeds were redissolved in toluene and stored inside a glovebox under nitrogen atmosphere.

Synthesis of CdSe/CdS Nanorods. The seeded growth method was employed to synthesize CdSe/CdS heterostructured nanorods.[34] Thus CdO (0.207 g), PPA (0.015 g), TOPO (2.0 g), and ODPA (1.28 g) were mixed in a three-neck flask. The solution was degassed, heated up to 150 °C, and kept under vacuum for 2 h. Then the solution was heated up to 340 °C and kept at that temperature for 15 min. Next, 1.5 g of TOP was injected. After stabilization at 340 °C, TOP-S solution (0.05152 g S + 0.5957 g TOP) and TOP-seeds solution (2 mg CdSe seeds +0.5 mL TOP) were rapidly injected in the flask. The reaction solution was kept at high temperature during 10 min, and then the reaction was quenched by injection of 5 mL of room-temperature toluene. After the synthesis, the CdSe/CdS nanorods were precipitated with methanol (20 mL) and were then redissolved in toluene (5 mL) containing dodecanoic acid (0.125 g) and octylamine (0.390 g). The CdSe/CdS nanorods were 70 nm long and 5.5 nm large in diameter.

Synthesis of Gold-Tipped CdSe/CdS Nanorods. The gold growth onto the tip of CdSe/CdS nanorods was performed by UV illumination of mixture of gold precursor and CdSe/CdS nanorods in toluene solution. The gold salt solution was prepared from a mixture of 10 mg of $AuCl_3$, 70 mg of dodecyldimethylammonium bromide (DDAB) and 50 mg of dodecylamine (DDA), dissolved in 10 mL of toluene and sonicated for 10 min until the solution turned to light yellow. Then, argon was bubbled in the solution for 5 min. Before the reaction, CdSe/CdS nanorods had been treated with dodecanoic acid in order to promote the gold growth only onto the tip of nanorods. 50 mg of dodecanoic acid and 1 mL of CdSe/CdS solution was mixed and kept under stirring for 1h. Then, the nanorod solution was washed twice with excess of ethanol and centrifugated. 200 μL of gold precursor solution and 200 μL of CdSe/CdS solution ($C = 1 \times 10^{-5}$ g/mol) were mixed in glass vial (lamp/sample distance of 150 mm) and illuminated by UV lamp (1mW/cm^2 power) for 60 min at room temperature under stirring. After the synthesis, the NPs were washed by adding acetone, precipitated by centrifugation and, finally redispersed in toluene. The experiment without UV illumination was followed the same procedures except that the reaction mixture was kept in the darkness to avoid exposure of the reaction mixture to UV or visible light.

Characterizations. The size and morphology of semiconductor/(metal) heterostructures were characterized by transmission electron microscopy (TEM; FEI Tecnai F20ST). Glass capillary containing 100 μL of nanorod/gold salt mixture was used in small-angle X-ray scattering (SAXS) experiments. After mixing of nanorod and gold salt solutions, defined as the zero point, the SAXS measurements had been carried out each 30 s until 3600 s. SAXS measurements were performed at 12-ID-C station at the Advanced Photon Source (ANL). X-ray energy was 12 KeV, which is corresponding to wavelength 1.0332 Å. The sample to detector distance was about 2 m. A 2D CCD detector was used to acquire images with typical exposure times in the range of 0.01−1 s. In-situ absorption measurements were performed using a UV broadband lamp and CCD for rapidly stirred solutions of nanorods in toluene. In situ PL decay measurements were recorded for rapidly stirred nanorod solutions in toluene solvent. Nanorods were excited at 2 kHz by 420 nm pulses from a 2 kHz amplified Ti:sapphire laser. The PL was collected with a lens and directed to a long pass filter and a 150 mm spectrograph, and detected with a photon-counting streak camera. It is worth mentioning that the UV exposure condition of samples did not negatively affect PL decay measurements despite additional PL from the sample. Ultrafast PL decay measurements were recorded using streak camera detection, but utilized RF phase locking electronics that provide increased temporal resolution. Ultrafast transient absorption measurements were carried out using an amplified Ti:sapphire laser (800 nm, 35 fs, 2 kHz repetition rate) the output of which was split into two beams. The first beam, containing 10% of the power, was focused into a sapphire window to generate a white light continuum (440 nm −750 nm), which serves as the probe. The other beam, containing 90% of the power, was sent into an optical parametric amplifier to generate the 420 nm pump beam. After passing through a depolarizer, the pump beam is focused and overlapped with the probe beam at the sample. The pump power was chosen to be 20 nJ/pulse; at these pump energies, we observed no power-dependent kinetic features corresponding to multiexciton decay, indicating that each nanorod absorbs on average less than one photon per pulse. Absorption spectra of the samples were found to be identical before and after the transient absorption (TA) experiments, indicating that the measurements condictions do not damage or alter the samples. X-ray spectroscopy measurements were performed at the 10-ID beamline at the Advanced Photon Source, Argonne National Laboratory. Measurements at the Au L3-edge (11919 eV) were performed on the samples in sealed cylindrical cuvettes in fluorescence mode using Lytle detector. Au foil was measured with help of the reference ion chamber for every scan taken on the samples. The standards were measured in transmission geometry. In situ TA, PL, and SAXS measurements were started immediately after introduction of the solution of gold precursor.

RESULTS AND DISCUSSION

Gold-tipped CdSe/CdS heterostructures were synthesized according to a modification of previously reported procedures developed for metals[35,36] and semiconductor NPs decorated with noble metal NPs.[10,37,38] Briefly, CdSe/CdS nanorods were

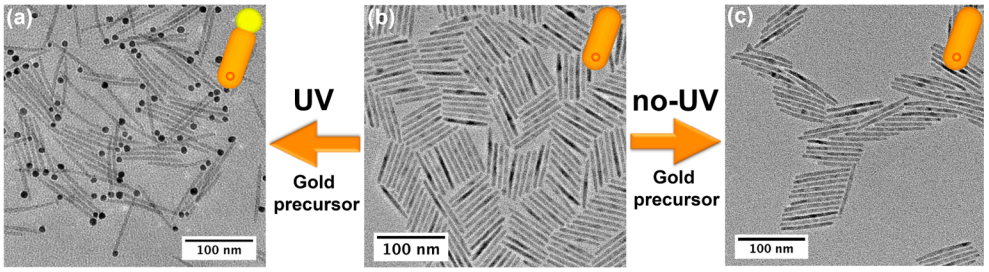

Figure 1. TEM images of CdSe/CdS nanorods (length L = 70 nm and diameter D = 5.5 nm) (b) with Au domains on their tips (diameter D = 9.5 nm) obtained under UV illumination (a) and CdSe/CdS nanorods exposed to Au precursor with no-UV illumination (c).

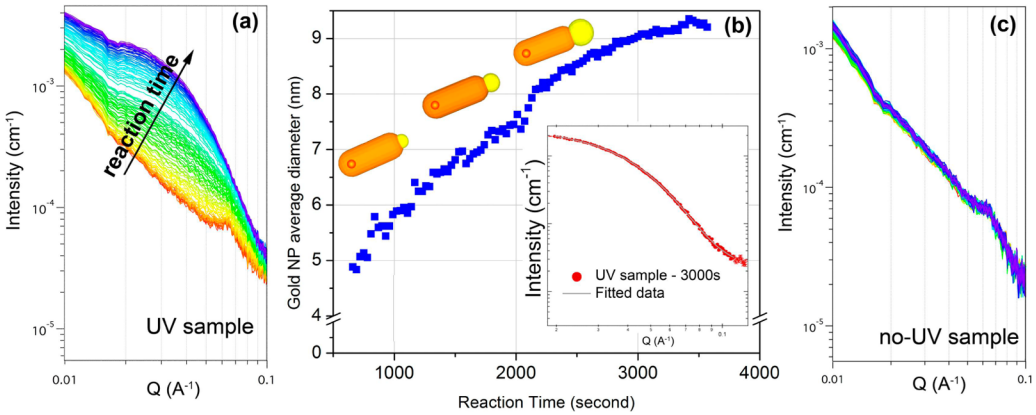

Figure 2. (a) Evolution of SAXS spectra recorded in situ of CdSe/CdS nanorods during nucleation and growth of Au domains under UV illumination for a reaction time range of 0−3600 s. (b) Evolution of the average size of Au domain as a function of the reaction time. Inset demonstrates the SAXS spectrum of CdSe/CdS/Au heterostructure normalized by the spectrum of initial CdSe/CdS and simulation curve obtained using Bessel function. (c) In situ SAXS data on CdSe/CdS and gold precursor mixture that was not exposed to UV illumination corresponding to the different reaction times.

prepared using a seeded growth method.[33,34,39,40] As shown in Figure 1, the average length and diameter of CdSe/CdS nanorods are L = 70 nm and D = 5.5 nm, respectively. Toluene solution of CdSe/CdS nanorods was mixed with a solution of gold(III) chloride ($AuCl_3$), didodecyldimethylammonium bromide (DDAB), and dodecylamine (HDA) and illuminated with UV at room temperature. After precipitating with acetone followed by centrifugation, Au-tipped CdSe/CdS nanorods were redispersed in toluene and stored in the darkness. Figure 1a shows the CdSe/CdS nanorods with ∼9.5 nm Au domains (stdv 10%) on the tip of each CdSe/CdS nanorod. Control experiments when the reaction mixture containing the same concentration of CdSe/CdS nanorods and Au precursor was kept in darkness confirmed no formation of Au domains on the semiconductor nanorods (Figure 1c). Lack of formation of Au on CdSe/CdS nanorods was further confirmed by HRTEM data (Figure S1). More details on the synthesis procedure are given in the Supporting Information.

To monitor the kinetics of the formation of Au domains on CdSe/CdS nanorods and further correlate the nucleation and growth of Au at the CdSe/CdS surface with the optical properties of the CdSe/CdS/Au heterosturtures, we performed synchrotron small-angle X-ray scattering (SAXS). The SAXS plots were obtained from radial averaging of two-dimensional scattering images over all orientations. The SAXS spectra were acquired each 30 s until the reaction was complete (∼3600 s). Figure 2 shows SAXS patterns, measured as a function of scattering vector q, for both UV and no-UV samples. At the early stages of the reaction, the SAXS spectra of the reaction mixture exhibit features characteristic to CdSe/CdS nanorods only. To extract the average diameter and number of Au domains, the SAXS spectra (following subtraction of the CdSe/CdS nanorod contribution) were fitted using a polydisperse sphere model (Figure 2b).[41] The inset in Figure 2b shows a good agreement between experimental SAXS data and the fitted curves obtained for the Au domains assuming their spherical shape (Figure S2). It is worth noting that the data fit quality is reliable only after ∼600 s of the reaction time, since at early reaction times, the size of Au domains is too small and their size distribution is too broad to be meaningfully fitted. The number of Au domains and their size distribution are shown in Figure S3. In control experiments, when the reaction mixture was not illuminated by UV, acquired SAXS data indicate a lack of discernible change during the same reaction period (Figure 2c), indicating no Au domains are formed on the tip of CdSe/CdS nanorods. Thus, SAXS data are in agreement with the TEM data shown in Figure 1.

The evolution of optical properties of CdSe/CdS nanorods mixed with the gold precursor (both UV and no-UV samples) were examined in situ by measuring the UV−visible absorption, PL intensity, and transient PL decay dynamics as a function of a reaction time. Figure 3 presents the time evolution of the absorption spectra of CdSe/CdS nanorods after introducing the gold precursor under UV illumination. Starting with the excitonic absorption of CdSe/CdS nanorods, with time, an additional broad peak develops at ∼575 nm that is consistent with the surface plasmon resonance of Au NPs. Notice, that the absorption near ∼450 nm increases during the photoreaction (by a factor two), corresponding to the superposition of the CdS band-edge transition and the interband transitions in the

dx.doi.org/10.1021/ja4092616 | J. Am. Chem. Soc. 2014, 136, 2342−2350

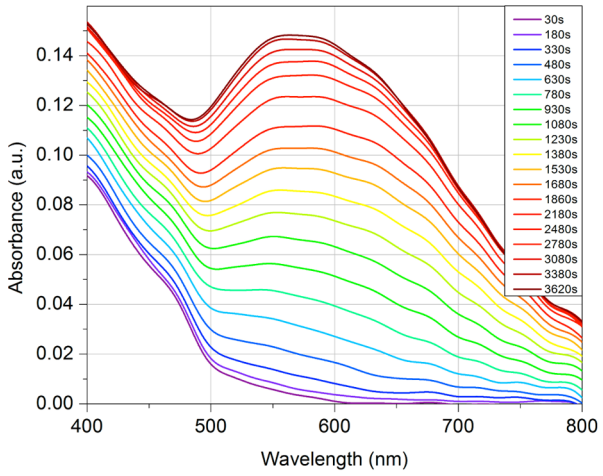

Figure 3. Evolution of the absorption spectra of CdSe/CdS nanorods reacted with the gold precursor under UV illumination as a function of the reaction time.

Au domain. The absorption spectra of CdSe/CdS nanorods mixed with the Au precursor but not illuminated with UV (no-UV samples) revealed no significant changes during the same time interval as UV samples (Figure S4). This confirms that no Au NPs large enough to produce a discernible surface plasmon resonance are formed when the reaction mixture is not illuminated with UV.

Next, we studied in situ time-resolved PL decays as a function of the reaction time after mixing the CdSe/CdS nanorods and Au precursor. PL decay dynamics were recorded every 30 s by weakly exciting the stirred samples with 50 μW of 3.0 eV photons produced by a 35 fs, 2 kHz Ti:sapphire laser. PL photons were spectrally dispersed and detected using a streak camera. For UV samples we found that the PL decay dynamics appeared highly single exponential subsequent to the first 3 ns after excitation (Figure 4a), and corresponds to the previously reported radiative relaxation time of the exciton associated with the CdSe/CdS semiconductor nanorods.[33,42,43] PL spectra of CdSe/CdS nanorods reacting with Au precursor under UV illumination and in the darkness are shown in Figures S5 and S6. No trap PL has been observed.

The faster initial PL decay prior to 3 ns likely corresponds to carrier trapping. Surprisingly, in the no-UV samples in which no Au domains were present, we observe similar evolution of the time-resolved PL behavior (Figure 4b). Figure S7 shows that the dynamic of the decay of initial amplitudes are very similar for UV and no-UV samples, meaning that in both samples a similar process is involved in carrier trapping. Examination of the time-integrated PL intensity as a function of reaction time also shows a close resemblance for both UV and no-UV samples (Figure 5) suggesting that the PL quenching of CdSe/CdS is irrespective of the presence of a Au tip. In order to rule out any effect of weak laser illumination used in PL decay measurements on no-UV samples, we performed a control experiment wherein the solution of CdSe/CdS nanorods mixed with gold precursor was kept in the darkness and measured only at the end points of the reaction (Figure 5). This control experiment confirmed that the visible laser excitation used to conduct PL decay measurements did not cause the formation of Au domains on the semiconductor nanorods under no-UV conditions.

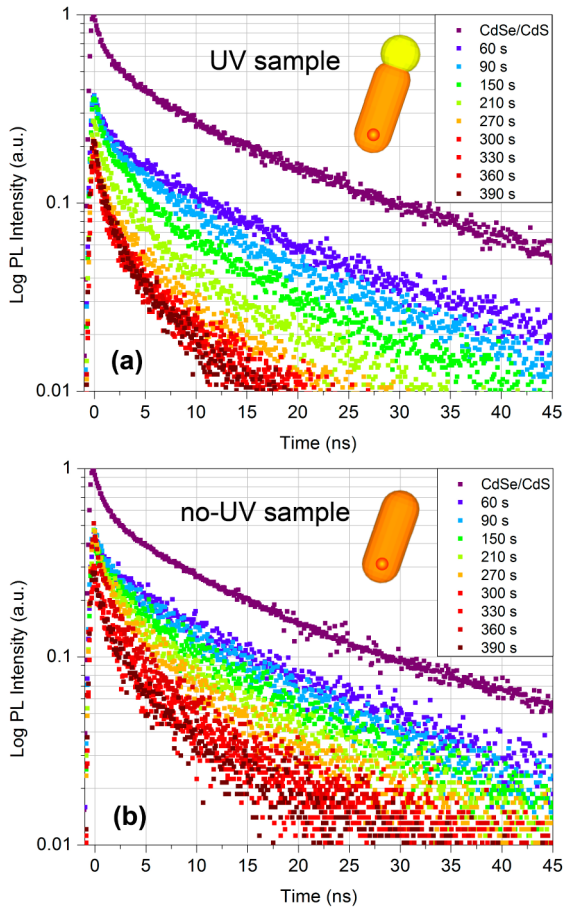

Figure 4. PL decays as a function of reaction time of CdSe/CdS nanorods with gold precursors (a) under UV irradiation and (b) under no-UV conditions.

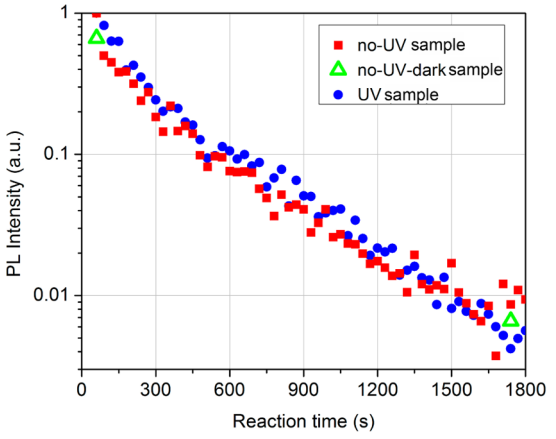

Figure 5. Time-integrated PL intensity as a function of the reaction time with gold precursor for UV and no-UV samples, respectively. Excitation wavelength was 420 nm. The green open symbols correspond to CdSe/CdSe nanorods mixed with gold precursor and kept in the darkness.

To further investigate the PL quenching of CdSe/CdS nanorods after introducing the Au precursor with and without UV illumination, we performed in situ ultrafast time-resolved PL measurements. Figure 6a and b displays a series of ultrafast PL decay dynamics as a function of the reaction time. Here, although the initial decay amplitude decreases, single

dx.doi.org/10.1021/ja4092616 | J. Am. Chem. Soc. 2014, 136, 2342−2350

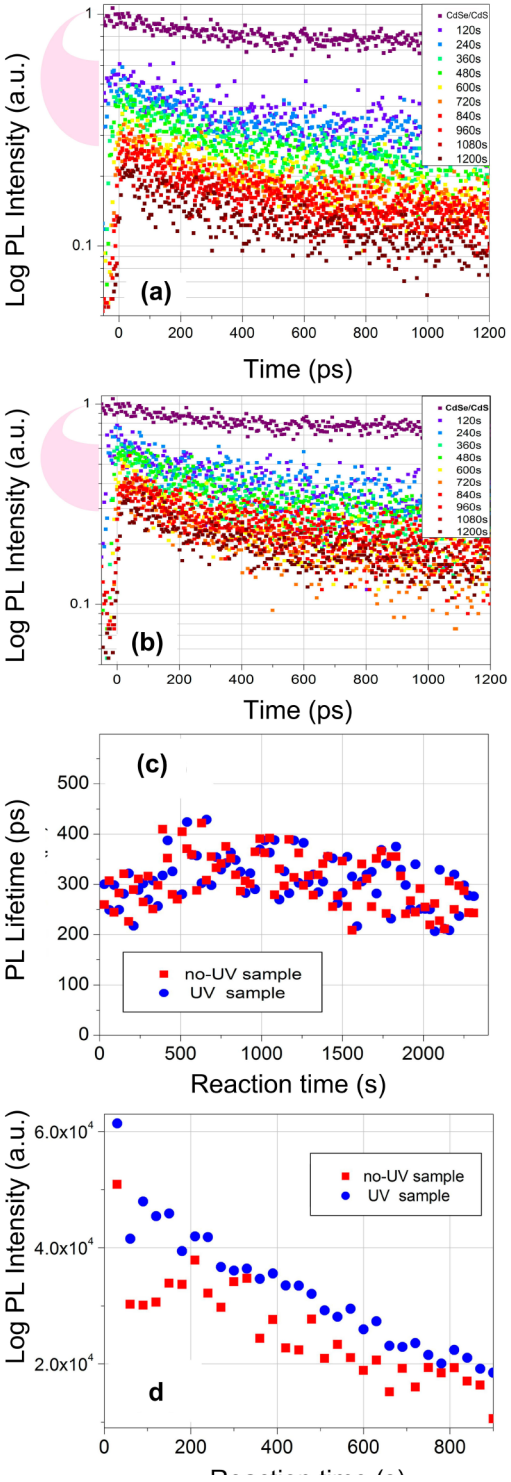

Figure 6. Ultrafast PL decay dynamics (excitation wavelength: 420 nm) as a function of reaction time of CdSe/CdS nanorods with Au precursor with and without UV illumination (a and b, respectively). (c) PL lifetimes for the UV and no-UV samples as a function of the reaction time. (d) Early time integrated PL intensities (0 to 1200 ps) for UV and no-UV samples as a function of the reaction time. The decrease of PL both in UV and no-UV samples on ps to sub-ps time scale is highlighted in (a) and (b) by pink arrows on the left.

exponential fitting reveals a fairly steady decay lifetime of ∼300 ps for both UV and no-UV samples (Figure 6c), associated with carrier trapping.[33] In similarity to Figure 5, the PL intensity plots as a function of reaction time again shows a similar decay profile for both samples (Figure 6d). Therefore, the ultrafast decay probing again shows no clear difference in terms of carrier kinetics for UV and no-UV samples. However, the decrease of the decay of the early time instantaneous PL intensity combined with the absence of a distinct decay process suggests that an unresolved, fast process such as charge transfer occurs on a single-picosecond to subpicosecond time scale (less than 3 ps − time resolution of the instrument). Such a value is consistent with previous data on Au-tipped CdS nanorods.[1,22] It is worth noticing that between the beginning and the end of the photoreaction, the PL intensity for the UV sample decreases by a factor of 5 (Figure 6d), whereas the absorption at the excitation wavelength is increased by ∼1.7x at 420 nm, as shown in Figure 3. This observation indicates that Au absorption does not govern the observed PL decay.

Next, to further investigate the charge transfer in the UV and no-UV samples, we performed femtosecond transient absorption spectroscopy using 420-nm excitation. Figure 7 presents transient spectra (TA) measured at a 1.5-ps pump−probe time delay for initial CdSe/CdS nanorods, as well as for CdSe/CdS nanorods with UV and no-UV illumination following their exposure (1800 s) to the gold precursor (for more details, see Figures S8 and S9). The Au-tipped nanorods (UV sample) show spectrally broad bleaching of the absorption band around $\lambda \sim 544$ nm, which corresponds to the surface plasmon resonance of spherical Au NPs. The transient absorption peak is slightly shifted in comparison to that observed in steady-state absorption (Figure 3), possibly due to some coupling to higher-pole oscillations (quadrapole, octapole).[44] The induced adsorption in the TA signal of the UV-sample is due to plasmon broaderning.[45] Each of the samples also shows a bleach feature near 475 nm, which corresponds to excitation of carriers in the CdS component of the nanorods.[33,42] It is worth mentioning that for II−VI semiconductor NPs the density of electron quantized states is significantly less as compared to the density of hole states.[46,47] As a result, TA measurements are sensitive to electrons but not to holes, whereas the PL-decay dynamics measurements described above are sensitive to semiconductor nanorods containing both carriers. Note, that TA data indicate the presence of electrons in CdS in all three samples at different delay times such as 1.5, 5, and even 20 ps. Furthermore, in the UV-sample, the CdS bleach feature is not due to the presence of unmodified CdSe/CdS nanorods since each semiconductor rod has Au domain, as is evidenced in Figure 1. As a result, the CdS bleach feature in the UV-sample indeed indicates the presence of electrons in CdS. We observe the shift of TA spectra of no-UV sample at 1.5 ps off the spectra of CdSe/CdS in the range from ∼540 to ∼575 nm. We believe that the fast hole transfer to surface species in the no-UV and UV sample can potentially impedes hot electron relaxation vs electron−hole energy transfer resulting in the shift of the higher energy bleaching signal. This process happens at ∼ps time scale since TA spectrum of no-UV sample at 5 ps does not reveal this feature (Figure 7). The broad plasmon feature in this spectral range hides this spectral detail of the TA spectrum of UV-sample. The difference below 520 nm between the no-UV and original CdSe/CdS samples TA spectra could arise from the charge separation of positively charged surface species formed after introduction of gold precursor and negatively charged CdSe/CdS. The significantly smaller CdS bleach in the UV-sample can be explained by overlap of this bleach with the Au plasmon band at 470 nm characteristic to interband or thermal

dx.doi.org/10.1021/ja4092616 | J. Am. Chem. Soc. 2014, 136, 2342−2350

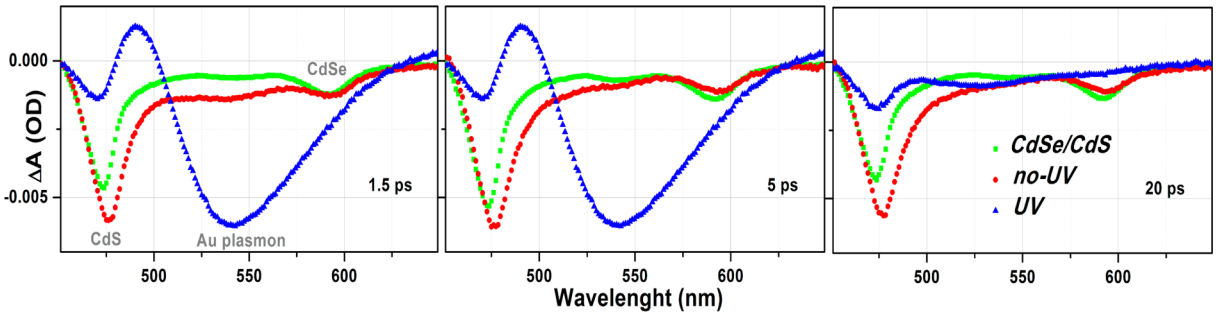

Figure 7. Transient absorption spectra measured at Δt = 1.5, 5, and 20 ps for original CdSe/CdS nanorods (green), exposed to gold precursor under UV (blue) and kept in the darkness (red) for 1800 s. Even though the UV sample shows strong bleach associated with the gold plasmon (centered near 544 nm), all of the samples exhibit bleaching near 475 and 585 nm, which can be respectively attributed to the presence of electrons in the CdS and CdSe components of each structure. ΔA has been normalized by the concentration of CdSe/CdS nanorods (addition of gold-ion containing solution dilutes the original nanorod sample).

redistribution of electrons below Fermi level.[44] If the 470 nm Au band is taken into account, the CdS bleach in the UV sample will exhibit intensity similar to the no-UV sample. Even though the CdSe bleach feature overlaps with Au plasmon, resulting in asymmetric peak in spectral range corresponding to surface plasmon peak and CdSe bleach feature, qualitative analysis of TA data at different delay times allows us to assume that the TA kinetics of CdSe bleach follows the TA kinetics of CdS bleach.

Figures 8 and S10 show similarity between the TA measurements for the pristine CdSe/CdS nanorods and the

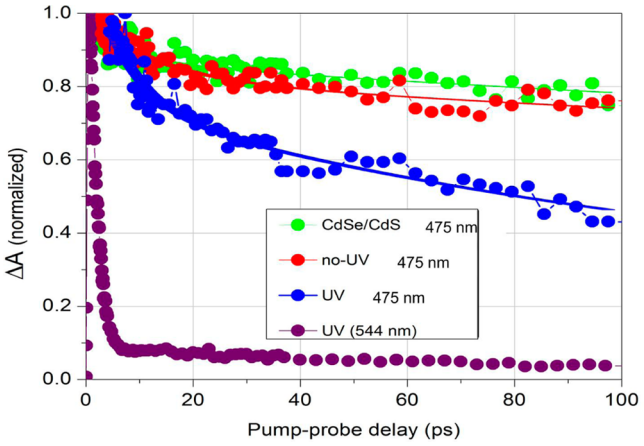

Figure 8. Transient absorption kinetics for CdSe/CdS nanorods, no-UV sample and UV sample at 475 nm (CdS bleach), and the UV sample at 544 nm corresponding to the gold plasmon peak.

no-UV sample, whereas some small loss of amplitude is apparent for the UV sample. The TA dynamics indicate that electrons do not rapidly leave the no-UV sample, and that some electron transfer from the UV sample likely does take place. Taken together with the fast, similar PL quenching temporal profiles observed for both UV and no-UV samples, these data suggest that rapid hole transfer leads to ultrafast PL quenching. The presence of substantial CdS bleach in CdSe/CdS/Au at times scales of hundreds of ps indicates that electron transfer in such systems takes at least more than tens of ps. More important, the control experiment with CdSe/CdS nanorods exposed to the solution of gold precursor demonstrates the same dynamics in PL quenching as CdSe/CdS/Au structures while, obviously, transient adsorption kinetics for these nanorods is very similar to the original CdSe/CdS sample. We conclude that indeed electron transfer takes place in the CdSe/CdS/Au system, however with a far slower time scale than the process that controls the PL quenching.

It is worth mentioning that, recently, an electron transfer time faster than 20 fs has been reported for CdS/Au NPs. This conclusion has been made based on the observed loss of CdS bleach in the CdS/Au samples at such time scales and analysis of the red shift of Au plasmon.[22] In contrast, our data indicate that in our study we do observe CdS bleach features at the time scales (e.g., 20 ps) at which no PL is observed in case of both UV and no-UV samples. The red shift of the plasmon we can also attribute to the higher dielectric constant of CdS that is in close proximity to the Au domain.

To quantify the decays shown in Figures 8 and S10, biexponential fits to the dynamics of electron trapping processes are shown in Table 1. Decay lifetimes, τ_1 and τ_2, describing the charge dynamics are similar for the pristine CdSe/CdS nanorods and the no-UV sample. The significantly faster τ_2 in the UV samples is suggestive of electron transfer from the semiconductor component to the Au domain, while τ_1, being very fast and fairly constant for all samples, is likely to be unrelated to the processes involving Au. The 1.7 ps decay time observed at 544 nm is consistent with direct excitation of the gold plasmon that inevitably occurs upon excitation of samples containing a gold domain.[48]

Table 1. Lifetimes (τ_1 and τ_2) Obtained from Transient Absorption Analysis for No-UV and UV Samples at the Reaction Time of 1800 s

sample	τ_1, ps	τ_2 ps
CdSe/CdS NRs, 475 nm	13.6 ± 1.4	349 ± 52
no-UV, 475 nm	12.7 ± 1.2	330 ± 49
UV, 475 nm	7.3 ± 1.5	133 ± 23
UV, 544 nm (plasmon)	1.71 ± 0.03	67.5 ± 7.1

Addition of methyl viologen (MV^{2+}), an electron scavenger, to no-UV and UV samples reduced the bleach at both 475 nm (CdS feature) and 595 nm (CdSe feature) on a <1 ps time scale (Figures S11, S12). The formation of MV^{+} from MV^{2+} upon photooxidation of CdSe/CdS is confirmed by an induced absorption at 595 nm characteristic to MV^{+}.[43] Thus, the electron transfer from the semiconductor nanorod to the electron scavenger happens at a faster time scale than electron transfer from the semiconductor nanorod to the gold domain.

dx.doi.org/10.1021/ja4092616 | J. Am. Chem. Soc. 2014, 136, 2342−2350

This observation confirms that electrons are efficiently ejected from the semiconductor nanorod.

To understand why the Au precursor leads to a significant PL quenching irrespective of the presence or absence of Au domains in contact with the CdSe/CdS nanorod, we performed extended X-ray absorption fine structure (EXAFS) measurements of Au L3-edge in the UV and no-UV samples and Au precursor to study the local structure around the Au atoms. The EXAFS data were fitted in *r*-space and are plotted using k2 weighted data (see Figures S13 and S14). The fit parameters are listed in Table S1, and the bond lengths and coordination numbers for the bonds generated by fitting the data are listed in Table S2. We found that the peaks at 2.4 and 3.2 Å corresponding to Au−Au bonds are significantly stronger in the UV sample where Au domain are present while intensities of the peaks corresponding to Au−Au bonds were very weak in the no-UV sample (Figure 9). Both UV and no-UV samples

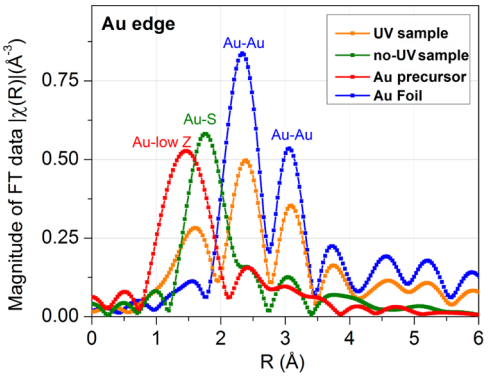

Figure 9. Fourier transformed EXAFS data in *r*-space for the Au edge measured for CdSe/CdS nanorod samples and reference samples such as Au foil and Au salt (Au^{3+}).

exhibit a pronounced peak at ∼1.7 Å that corresponds most likely to Au−S bonds, indicating a presence of Au−S bonds in both samples.[49] The coordination number for Au−Au bonds in the UV sample is less than 12 due to the nanoscale size of the samples, and the bond lengths are shorter than the bulk gold bond length of 2.88 Å.[50] Compared to the UV sample, we observe that the no-UV samples has very few Au−Au correlations similar to the Au−Au correlations observed in the Au precursor (Table S1) indicating the absence of extended metallic Au domains in the no-UV sample. Control EXAFS experiment on the Au precursor demonstrates that Au atoms are coordinated with low-Z elements (most likely nitrogen as a result of the formation of complexes with DDAB and DDA molecules), as is evidenced from a peak at ∼1.5 Å visible in the low-R region corresponding to bond length of 1.96 Å (Table S1). The more expanded Au−Au bonds in the no-UV sample as compared with UV sample may result from Au bonding through S atoms (Table S1, Figures S14 and S15). X-ray absorption near edge spectroscopy (XANES) indicates that the spectrum of the Au standard is similar to the spectrum of the UV sample, meaning that the majority of gold present in this sample is represented by metallic gold (Figure 10). Linear combination fit analysis of XANES data for UV samples indicates that ∼70% of the correlations belong to Au−Au bonds, ∼2% to Au−Cl with Au^{3+}, and ∼28% to Au−S bonds with Au^{+} (Figure S15). XANES spectrum of the no-UV sample at the Au L3 edge is almost identical to the spectrum of the Au_2S standard (Figure 9), indicating that in the no-UV sample

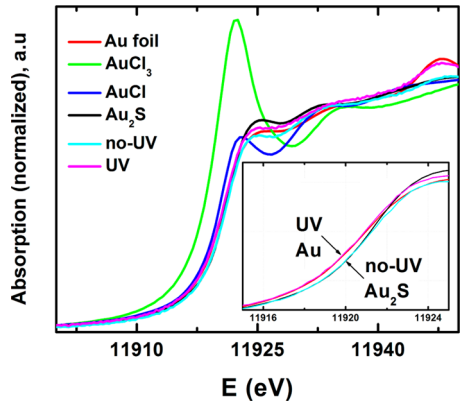

Figure 10. Au L3-edge XANES spectra of UV and no-UV samples; Au foil, $AuCl_3$, AuCl, and Au_2S standards. The inset magnifies the pre-edge region.

Au is mainly coordinated with sulfur. Linear combination fit analysis of XANES data on no-UV samples indicates ∼23% correlations belong to Au−Au bonds, ∼58% to Au−Cl with Au^{+}, and ∼19% to Au−S correlations with Au^{+} (Figure S15). A high number, at first glance, of Au−Au correlations in the no-UV samples is due to Au−Au bonds characteristic of Au_2S. Thus, fitting of EXAFS data at Au edge from standard Au_2S indicated 1.8 (0.2) Au−S bonds at 2.3 Å and 8 Au−Au bonds at 3.7 Å (Figure S16).

We assume that dodecylamine, present in the reaction mixtures of the UV and no-UV samples, can reduce Au^{3+} precursor to Au^{+} and no photoexcited electrons are needed to form Au(I)-S species. However, the formation of extended metallic gold domains happens at the expense of photoexcited electrons that are supplied from the semiconductor nanorods since the Au/CdSe/CdS hybrids are formed under light illumination only. In the reaction mixture, the only source of sulfur is the surface of the CdSe/CdS nanorods. Thus we can conclude that the surface of CdSe/CdS nanorods in UV and no-UV samples is covered with Au(1+)-S species. Precipitation of CdSe/CdS nanorods exposed to gold precursor with acetone followed with subsequent centrifugation and redispersion of CdSe/CdS nanorods in toluene does not recover the PL suggesting strong adsorption of Au(1+)-S at the surface of CdSe/CdS nanorods. High intensity of the signal corresponding to Au−S correlations in no-UV sample (Figure 9) suggests that Au(1+)-S species are formed not only on the CdSe/CdS tips, but are most likely also located on the sides of the nanorods. It is worth mentioning that the formation of surface species that can trap holes can facilitate the nucleation of Au at the nanorod surface since it prevents charge carrier recombination.[15]

■ CONCLUSIONS

In summary, we have shown that PL quenching in semiconductor/metal heterostructures is consistent with rapid hole transfer to gold−sulfur sites at the surface of semiconductor NPs. Also, this PL quenching process predominantly takes place on fast (less than 3 ps) time scales regardless of the presence or absence of the Au domains on the CdSe/CdS semiconductor if semiconductor nanorods have been exposed to the gold precursor. The electron transfer takes place in the CdSe/CdS/Au system, however, at far slower time scale than the process responsible for the PL quenching, and as a result we conclude that indeed hole transfer is responsible for the PL

dx.doi.org/10.1021/ja4092616 | J. Am. Chem. Soc. 2014, 136, 2342−2350

quenching. Surprisingly, this dominant quenching mechanism has been overlooked in previous end point studies on semiconductor/metal heterostructures. Our observation emphasizes the importance of in situ studies. This work suggests that exposure of semiconductor NPs to metal ions can play a significant role electronically and that structural characterization of hybrid semiconductor-metal materials does not convey the material behavior. We expect that the kinetic of PL quenching of semiconductor NPs exposed to different types of metal ions can be utilized in their detection.

■ ASSOCIATED CONTENT

Supporting Information

HRTEM of CdSe/CdS treated with gold precursors. SAXS data and fits for different reaction times. Evolution of Au NP number and size distribution as a function of the reaction time of CdSe/CdS and gold precursor under UV illumination. Absorption and PL spectra of CdSe/CdS exposed to gold precursor in the darkness (no-UV sample) as a function of the reaction time. TA spectra of CdSe/CdS nanorods, UV and no-UV samples. TA kinetics data for CdSe/CdS nanorods, no-UV and UV samples. Data on the effect of electron scavengers on TA of CdSe/CdS nanorods treated with gold precursor. Details on the EXAFS and XANES measurements. This material is available free of charge via the Internet at http://pubs.acs.org.

■ AUTHOR INFORMATION

Corresponding Authors

schaller@anl.gov
eshevchenko@anl.gov

Notes

The authors declare no competing financial interest.

■ ACKNOWLEDGMENTS

Use of the Center for Nanoscale Materials, Advanced Photon Source, and Electron Microscopy Center, was supported by the U.S. Department of Energy, Office of Science, Office of Basic Energy Sciences, under Contract No. DE-AC0206CH- 11357. The authors would like to thank Prof. Carlo Segre of Illinois Institute of Technology for staff time used to perform the EXAFS experiments and to Dr. Vladislav Zyryanov for designing sample cells used for EXAFS samples. MRCAT operations are supported by the Department of Energy and the MRCAT member institutions. Use of the Advanced Photon Source, an Office of Science User Facilities operated for the U.S. Department of Energy (DOE) Office of Science by Argonne National Laboratory, was supported by the U.S. DOE under Contract No. DE-AC02-06CH11357.

■ REFERENCES

(1) Wu, K.; Zhu, H.; Liu, Z.; Rodríguez-Córdoba, W.; Lian, T. *J. Am. Chem. Soc.* **2012**, *134*, 10337−10340.
(2) Carbone, L.; Cozzoli, P. D. *Nano Today* **2010**, *5*, 449−493.
(3) Costi, R.; Saunders, A. E.; Banin, U. *Angew. Chem., Int. Ed.* **2010**, *49*, 4878−4897.
(4) Mokari, T.; Sztrum, C. G.; Salant, A.; Rabani, E.; Banin, U. *Nat. Mater.* **2005**, *4*, 855−863.
(5) Carbone, L.; Jakab, A.; Khalavka, Y.; Soennichsen, C. *Nano Lett.* **2009**, *9*, 3710−3714.
(6) Korobchevskaya, K. G. C.; Manna, L.; Comin, A. *J. Phys. Chem. C* **2012**, *116*, 26924−26928.
(7) Costi, R.; Saunders, A. E.; Elmalem, E.; Salant, A.; Banin, U. *Nano Lett.* **2008**, *8*, 637−641.
(8) Yin, H.; et al. *Chem. Commun.* **2008**, 4357−4359.
(9) Acharya, K. P.; et al. *Nano Lett.* **2011**, *11*, 2919−2926.
(10) Menagen, G.; Macdonald, J. E.; Shemesh, Y.; Popov, I.; Banin, U. *J. Am. Chem. Soc.* **2009**, *131*, 17406−17411.
(11) Wang, C.; Yin, H. F.; Dai, S.; Sun, S. H. *Chem. Mater.* **2010**, *22*, 3277−3282.
(12) Wang, D.; Li, X.; Li, H.; Li, L.; Hong, X.; Peng, Q.; Li, Y. *J. Mater. Chem. A* **2013**, *1*, 1587−1590.
(13) Kamat, P. *J. Phys. Chem. C.* **2008**, *112*, 18737−18753.
(14) Amirav, L.; Alivisatos, A. P. *J. Phys. Chem. Lett.* **2010**, *1*, 1051−1054.
(15) Amirav, L. A.; Alivisatos, A. P. *J. Am. Chem. Soc.* **2013**, *135*, 13049−11305.
(16) Zhu, H.; Song, N.; Lv, H.; Hill, G. L.; Lian, T. *J. Am. Chem. Soc.* **2012**, *134*, 11701−11708.
(17) Berr, M. J.; Vaneski, A.; Mauser, C.; Fischbach, S.; Susha, A. S.; Rogach, A. L.; Jäckel, F.; Feldmann, J. *Small* **2012**, *8*, 291−297.
(18) Shaviv, E.; Schubert, O.; Alves-Santos, M.; Goldoni, G.; Felice, R. Di; Vallée, F.; Fatti, N. Del; Banin, U.; Sönnichsen, C. *ACS Nano* **2011**, *5*, 4712−4719.
(19) Zhou, H.; Qu, Y.; Zeid, T.; Duan, X. *Energy Environ. Sci.* **2012**, *5*, 6732−6743.
(20) Tongying, P.; Plashnitsa, V. V.; Petchsang, N.; Vietmeyer, F.; Ferraudi, G. J.; Krylova, G.; Kuno, M. *J. Phys. Chem. Lett.* **2012**, *3*, 3234−3240.
(21) Saunders, A. E.; Popov, I.; Banin, U. *J. Phys. Chem. B* **2006**, *110*, 25421−25429.
(22) Mongin, D.; Shaviv, E.; Maioli, P.; Crut, A.; Banin, U.; Fatti, N. Del; Vallée, F. *ACS Nano* **2012**, *6*, 7034−7043.
(23) Khon, E.; Mereshchenko, A.; Tarnovsky, A. N.; Acharya, K.; Klinkova, A.; Hewa-Kasakarage, N. N.; Nemitz, I.; Zamkov, M. *Nano Lett.* **2011**, *11*, 1792−1799.
(24) Subramanian, V.; Wolf, E. E.; Kamat, P. V *J. Am. Chem. Soc.* **2004**, *126*, 4943−4950.
(25) Vaneski, A.; Susha, A. S.; Rodríguez-Fernández, J.; Berr, M.; Jäckel, F.; Feldmann, J.; Rogach, A. L. *Adv. Funct. Mater.* **2011**, *21*, 1547−1556.
(26) Gattás-Asfura, K. M.; Leblanc, R. M. *Chem. Commun.* **2003**, 2684−2685.
(27) Hsu, Y.; Lu, S.; Lin, Y. *Chem. Mater.* **2008**, 2854−2856.
(28) Mandal, A.; Dandapat, A.; De, G. *Analyst* **2012**, *137*, 765−772.
(29) Aberasturi, D. J. De; Montenegro, J.; Larramendi, I. R. De; Rojo, T.; Klar, T. A.; Alvarez-puebla, R.; Liz-Marzan, L. M.; Parak, W. J. *Chem. Mater.* **2012**, *24*, 738−745.
(30) Ma, Q.; Su, X. *Analyst* **2011**, *136*, 4883−4893.
(31) Elmalem, E.; Saunders, A. E.; Costi, R.; Salant, A.; Banin, U. *Adv. Mater.* **2008**, *20*, 4312−4317.
(32) Buck, M. R.; Bondi, J. F.; Schaak, R. E. *Nat. Chem.* **2012**, *4*, 37−44.
(33) She, C.; Demortière, A.; Shevchenko, E. V; Pelton, M. *J. Phys. Chem. Lett.* **2011**, *2*, 1469−1475.
(34) Talapin, D. V.; Koeppe, R.; Götzinger, S.; Kornowski, A.; Lupton, J. M.; Rogach, A. L.; Benson, O.; Feldmann, J.; Weller, H. *Nano Lett.* **2003**, *3*, 1677−1681.
(35) Krylova, G.; Giovanetti, L. J.; Requejo, F. G.; Dimitrijevic, N. M.; Prakapenka, A.; Shevchenko, E. V. *J. Am. Chem. Soc.* **2012**, *134*, 4384−4392.
(36) Pellegrino, T.; Fiore, A.; Carlino, E.; Giannini, C.; Cozzoli, P. D.; Ciccarella, G.; Respaud, M.; Palmirotta, L.; Cingolani, R.; Manna, L. *J. Am. Chem. Soc.* **2006**, *128*, 6690−6698.
(37) Menagen, G.; Mocatta, D.; Salant, A.; Popov, I.; Dorfs, D.; Banin, U. *Chem. Mater.* **2008**, *20*, 6900−6902.
(38) Li, X.; Lian, J.; Lin, M.; Chan, Y. *J. Am. Chem. Soc.* **2011**, *133*, 672−675.
(39) Carbone, L.; Nobile, C.; De Giorgi, M.; Sala, F. D.; Morello, G.; Pompa, P.; Hytch, M.; Snoeck, E.; Fiore, A.; Franchini, I. R.; Nadasan, M.; Silvestre, A. F.; Chiodo, L.; Kudera, S.; Cingolani, R.; Krahne, R.; Manna, L. *Nano Lett.* **2007**, *7*, 2942−2950.

(40) Talapin, D. V.; Nelson, J. H.; Shevchenko, E. V.; Aloni, S.; Sadtler, B.; Alivisatos, A. P. *Nano Lett.* **2007**, *7*, 2951−2959.
(41) X Xia, Y.; Nguyen, T. D.; Yang, M.; Lee, B.; Santos, A.; Podsiadlo, P.; Tang, Z.; Glotzer, S. C.; Kotov, N. *Nat. Nanotechnol.* **2011**, *6*, 580−587.
(42) Wu, K.; Rodríguez-Córdoba, W. E.; Liu, Z.; Zhu, H.; Lian, T. *ACS Nano* **2013**, *7*, 7173−7185.
(43) Dworak, L.; Matylitsky, V. V.; Breus, V. V.; Braun, M.; Basché, T.; Wachtveitl, J. . *J. Phys. Chem. C* **2011**, *115*, 3949−3955.
(44) Ahmadi, T. S.; Logunov, S. L.; El-Sayed, M. A. *J. Phys. Chem.* **1996**, *100*, 8053−8056.
(45) Logunov, S. L.; Ahmadi, T. S.; El-Sayed, M. A.; Khoury, J. T.; Whetten, R. L. *J. Phys. Chem. B* **1997**, *101*, 3713−3719.
(46) Malko, A. V.; Mikhailovsky, A. A.; Petruska, M. A.; Hollingsworth, J. A.; Klimov, V. I. *J. Phys. Chem. B* **2004**, *108*, 5250−5255.
(47) Klimov, V. I. *Annu. Rev. Phys. Chem.* **2007**, *58*, 635−673.
(48) Hodak, J.; Martini, I.; Hartland, G. V. *Chemi. Phys. Lett.* **1998**, *284*, 135−141.
(49) Crespo, P.; Litrán, R.; Rojas, T.; Multigner, M.; la Fuente, J. de; Sánchez-López, J.; García, M.; Hernando, A.; Penadés, S.; Fernández, A. *Phys. Rev. Lett.* **2004**, *93*, 087204.
(50) Miller, J. T.; Kropf, A. J.; Zha, Y.; Regalbuto, J. R.; Delannoy, L.; Louis, C.; Bus, E.; van Bokhoven, J. *J. Catal.* **2006**, *240*, 222−234.